Ilamycin E and ilamycin F are dual inhibitors of ClpX and ClpC1 in mycobacteria

Yamin Gao[1,2,3,4#], Cuiting Fang[1,2,3,4#], Biao Zhou[1,5,6], H.M. Adnan Hameed[1,2,3,4], Changli Sun[3,7], Xirong Tian[1,2,3,4], Jing He[1,2,4,8], Xingli Han[1,2,3,4], Han Zhang[1,2,4,9], Jianhua Ju[3,7], Xinwen Chen[6], Nanshan Zhong[6], Junying Ma[3,7*], Xiaoli Xiong[1,2,3,6*], Tianyu Zhang[1,2,3,4,6*]

[1] State Key Laboratory of Respiratory Disease, Guangzhou Institutes of Biomedicine and Health, Chinese Academy of Sciences, Guangzhou 510530, China

[2] Guangdong-HongKong-Macau Joint Laboratory of Infectious Respiratory Diseases, Guangzhou Institutes of Biomedicine and Health, Chinese Academy of Sciences, Guangzhou 510530, China

[3] University of Chinese Academy of Sciences, Beijing 100049, China

[4] China-New Zealand Belt and Road Joint Laboratory on Biomedicine and Health, Guangzhou Institutes of Biomedicine and Health, Chinese Academy of Sciences, Guangzhou 510530, China

[5] Guangzhou Medical University, Guangzhou 510180, China

[6] Guangzhou National Laboratory, Guangzhou 510005, China

[7] CAS Key Laboratory of Tropical Marine Bio-Resources and Ecology, Guangdong Key Laboratory of Marine Materia Medica, RNAM Center for Marine Microbiology, South China Sea Institute of Oceanology, Chinese Academy of Sciences, Guangzhou 510301, China.

[8] Institute of Physical Science and Information Technology, Anhui University, Hefei 230601, China

[9] School of Life Sciences, University of Science and Technology of China, Hefei 230026, China

[#] These authors contributed equally to this work.

[*]Corresponding authors: Tianyu Zhang (Tel: +86-20-32015270, E-mail: zhang_tianyu@gibh.ac.cn); Xiaoli Xiong (Tel: +86-20-32015327, E-mail: xiong_xiaoli@gibh.ac.cn); Junying Ma (Tel: +86-20-34066449, Email: majunying@scsio.ac.cn).

Abstract

The Clp protease system, which is crucial for maintaining protein homeostasis in mycobacteria, has become a promising target. Numerous non-ribosomal natural cyclic peptides, including ilamycins, have been reported to possess antitubercular activities by targeting the ClpC1 component of the ClpC1P1P2 proteasome. In this study, we found that ilamycin E and F (ILE/F) exhibit significantly more potent mycobactericidal activities than other ilamycin components by targeting both ClpX and ClpC1 components of the ClpC1P1P2 and ClpXP1P2 complexes. To our knowledge, this is the first report on the killing of mycobacteria by compounds through the targeting of ClpX. ILE/F have delayed antimicrobial activities and show synergistic or additive activities with many antituberculosis drugs against *Mycobacterium tuberculosis*, which is consistent with their mechanisms of action. Novel insertion mutations in *clpC1*, in addition to previously reported mutations, and a unique mutation in *clpX* have been identified and proven to cause resistance to ILE/F in mycobacteria. ILE markedly impedes the proteolytic function of the ClpC1P1P2 complex and may disrupt the function of the ClpXP1P2 complex by binding to ClpX. ILE/F are highly effective against mycobacteria by targeting both the ClpC1P1P2 and ClpXP1P2 complexes, highlighting the Clp complexes as promising potent targets, especially through a dual-targeting strategy.

Introduction

Mycobacteria are classified into three primary categories: the *Mycobacterium tuberculosis* (Mtb) complex, *Mycobacterium leprae* and non-tuberculous mycobacteria (NTM). Among these, tuberculosis (TB), which is caused by Mtb, continues to pose a significant global public health threat, with the situation being exacerbated by the emergence of drug-resistant Mtb strains[1,2]. Infections caused by NTM, such as *Mycobacterium abscessus* (Mab), are on the rise due to intrinsic resistance to almost all the existing antibiotics, and in several countries, the incidence of NTM infections has surpassed that of TB[3,4]. Consequently, there is an urgent need to discover and develop new drugs with novel mechanisms of action against drug-resistant mycobacteria to effectively manage mycobacterial diseases.

The caseinolytic protease (Clp) proteolytic system in mycobacteria has recently emerged as a promising therapeutic target[5-8]. This system is pivotal not only for maintaining intracellular protein quality but also for modulating responses to environmental stressors and contributing to the pathogenicity of virulent strains[6,9]. It comprises multi-subunit protein complexes that facilitate intracellular protein degradation. In mycobacteria, the core complex of the hetero-tetradecamer Clp protease assumes a barrel-shaped structure, constructed from two rings, each composed of seven ClpP1 and seven ClpP2 peptidase subunits. The entry of substrates into the ClpP1P2 complex is stringently regulated and reliant on ATP-dependent AAA+ unfoldases (ClpX or ClpC1), which act as adaptors to facilitate substrate entry into the protease chamber through ATP hydrolysis[8,10,11]. Both the Clp protease genes and the ATPase adaptor genes *clpX* and *clpC1* have been found essential for mycobacterial survival[8,12].

Many non-ribosomal natural cyclic peptides, such as ilamycins (also known as rufomycins), cyclomarins, ecumicins, and lassomycin, have been reported to possess antitubercular activities by targeting the ClpC1 component of the ClpC1P1P2 proteasome[13,14]. Although these compounds all disrupt protein metabolism through the Clp system, their mechanisms of action (MOAs) differ. For example, rufomycin I

decreases the proteolytic activity of the ClpP1P2 complexes by binding to ClpC1, interfering with its binding to ClpP1P2, while cyclomarin stimulates ClpC1's ATPase and promotes proteolysis by the ClpC1P1P2 proteasome[15,16]. Ecumicin and lassomycin, on the other hand, stimulate the ATPase activity of ClpC1 but inhibit the proteolysis by ClpP1P2[14,17]. To the best of our knowledge, there are no reported anti-Mtb compounds targeting ClpX.

We previously reported that ilamycin E (ILE) and ilamycin F (ILF), synthesized by *Streptomyces atratus* SCSIO ZH16 isolated from the South China Sea, exhibited activity against Mtb[18]. Particularly, ILE demonstrated superior activity against Mtb compared to other ilamycin components and the aforementioned compounds[13,14,18,19]. However, their MOAs, activities against NTM and other non-mycobacterial pathogenic bacteria, and potential drug interactions remain to be elucidated. In this study, we have discovered that ILE and ILF (ILE/F) exhibits high activity against Mtb by targeting both the ClpC1P1P2 and ClpXP1P2 complexes. This finding underscores the potential of Clp complexes as viable therapeutic targets, particularly when employing a dual-targeting approach.

Results

The selective and potent *in vitro* and *ex vivo* antimycobacterial activities of ILE/F

Mtb and 3 different NTM (Mab; *Mycobacterium marinum*, Mmr; *Mycobacterium smegmatis*, Msm) were selected to investigate the activities of ILE/F. These mycobacteria were chosen due to their clinical relevance and growth characteristics. Mab, a rapidly growing mycobacterium, is frequently associated with severe human infections[20] and is known for its intrinsic antibiotic-resistant nature[21]. Mmr, a slowly growing mycobacterium, is closely related to Mtb[22] but less virulent and serves as a model organism for Mtb studies[23]. Msm is also utilized widely as a model organism due to its rapid growth, non-virulence and the availability of genetic tools[23].

ILE/F demonstrated significant inhibitory activities against Mtb, Mmr, and Msm with varying potencies (Table 1). Notably, ILE exhibited potent activity against Mab at a concentration of 1 μg mL^{-1}, whereas ILF only showed weak activity at 20 μg mL^{-1}. This disparity in efficacy may stem from ILE/F structural differences and the unique cell wall permeabilities of each mycobacterial species[24,25]. Compared to rifampicin (RIF), ILE and ILF exhibited delayed antimicrobial activities, initially displaying minor bacteriostatic effects on Mtb, with bactericidal activity emerging after six days of incubation (Fig. 1). Similar killing dynamics were observed for Mab, Mmr, and Msm (Supplementary Fig. 1). The minimal inhibitory concentrations (MICs) of ILE against clinically isolated drug-resistant Mtb strains ranged from 0.01 to 0.05 μg mL^{-1}, which aligns with the laboratory standard Mtb $H_{37}Rv$ strain (Table 1). Synergistic effects were observed when combining ILE with RIF or the novel anti-TB drug TB47[26], currently a pre-investigational new drug, and when combining ILF with isoniazid (INH) or TB47. Partial synergy was noted when ILE was paired with INH, ethambutol (EMB), clofazimine (CLF), or bedaquiline (BDQ), and when ILF was combined with CLF. Additive effects were observed when ILE was combined with streptomycin (STR), or ILF combined with EMB, STR or BDQ. No antagonism was detected between any of the selected drugs and either ILE or ILF. In mouse

RAW264.7 macrophages, ILE effectively inhibited autoluminescent Mtb $H_{37}Rv$ (AlRv), with an MIC of 0.2 μg mL^{-1}. However, neither ILE nor ILF exhibited activity against common non-mycobacterial clinical isolates, with MICs exceeding 128 μg mL^{-1} (Table 1).

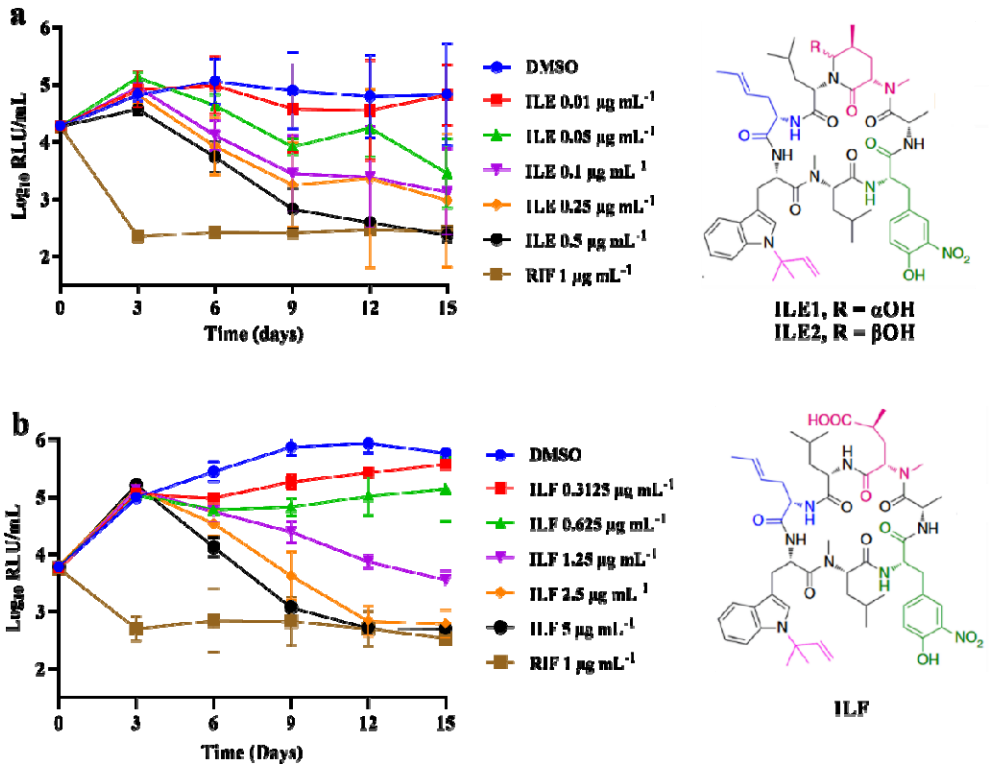

Fig. 1 | Time-kill curves of ILE/F against autoluminescent Mtb $H_{37}Ra$ (AlRa) and their structures. a Time-kill curves of ILE against AlRa and its structure. **b** Time-kill curves of ILF against AlRa and and its structure. The MIC_{lux} was defined as the lowest concentration that can inhibit > 90% relative light units (RLUs) compared with that from the untreated controls. DMSO, dimethyl sulfoxide, solvent control; RIF, positive control.

Table 1 | ILE/ILF spectrum of activities

Strains or drug combinations	ILE MIC (μg mL^{-1})	ILF MIC (μg mL^{-1})	FICI
AlRa	0.05[a]	1.25[a]	-
AlRv	0.05[a]	-	-
AlMsm	0.0625[a]	2.5[a]	-
AlMab	1[a]	20[a]	-
AlMmr	0.08[a]	0.625[a]	-
$H_{37}Rv$	0.025[b]	2.5[b]	-

K11*	0.025-0.05[b]	-	-
K12*	0.025[b]	-	-
K13*	0.01[b]	-	-
K14*	0.01[b]	-	-
K16*	0.05[b]	-	-
K17*	0.01[b]	-	-
K18*	0.025-0.05[b]	-	-
K19*	0.01[b]	-	-
K20*	0.05[b]	-	-
Staphylococcus aureus	> 128	> 128	-
Acinetobacter baumannii	> 128	> 128	-
Enterococcus faecium	> 128	> 128	-
Klebsiella pneumoniae	> 128	> 128	-
Pseudomonas aeruginosa	> 128	> 128	-
ILE + RIF	-	-	0.3125[a]
ILE + INH	-	-	0.625[a]
ILE + EMB	-	-	0.5625[a]
ILE + STR	-	-	1[a]
ILE + CLF	-	-	1[a]
ILE + BDQ	-	-	0.62[a]
ILE + TB47	-	-	0.3125[a]
ILF + RIF	-	-	1.0625
ILF + INH	-	-	0.3125
ILF + EMB	-	-	1
ILF + STR	-	-	1
ILF + CLF	-	-	0.63[a]
ILF + BDQ	-	-	1[a]
ILF + TB47	-	-	0.3125

AlRv, autoluminescent Mtb $H_{37}Rv$; AlMsm, autoluminescent Msm; AlMab, autoluminescent Mab; AlMmr, autoluminescent Mmr; FICI, fractional inhibitory concentration index; *, clinical resistant Mtb; [a], MICs obtained by detection of relative light units; [b], MICs obtained by the microplate alamar blue assay (MABA) method.

Mutation patterns in *clpC1* and/or *clpX* in ILE- or ILF-resistant Mtb, Mab, Msm, and Mmr mutants

The spontaneous mutation rate for producing ILE-resistant Mtb was approximately 2.5×10^{-9}, which is similar to that of rufomycin and lower than that of ecumicin and lassomycin, as well as RIF[14,15,17,27]. Whole genome sequencing (WGS) analysis revealed predominant mutations at P30 of ClpX and F80 of ClpC1 in ILE-resistant Mtb strains (Table 2). Similarly, ILE-resistant Mab exhibited mutations at the same site in ClpX and different sites in ClpC1, including F2, Q17, H77, L88, and an insertion between M1 and F2, resulting in an M1-FERF-F2 sequence (Table 2).

However, ILE-resistant Mmr strains carried mutations exclusively in ClpC1 without any mutations in ClpX (Table 2). Additionally, ILF-resistant Msm mutants showed mutations only in ClpC1, at F2, F5, F80, L88, I197, and an insertion between M1 and F2, leading to an M1-L-F2 sequence (Table 2), respectively. Cross-resistance between ILE and ILF was observed in all ILE- or ILF-resistant NTM mutants. These findings suggest that ILE/F may both target the ClpX and ClpC1.

Table 2 | Mutations of ClpC1 and ClpX in ILE- and ILF-resistant mutants

Strains No.	**Drug/MICs (μg mL^{-1})**	**Mutation in ClpC1**	**Mutation in *clpC1***	**Mutation in ClpX**	**Mutation in *clpX***
Mtb$^{R1\#}$	ILE 0.625	-	-	P30H	CCC→CAC
Mtb$^{R2\#}$	ILE 20	F80I	TTT→ATT	P30H	CCC→CAC
Mtb$^{R3\#}$	ILE 20	F80V	TTT→GTT	P30H	CCC→CAC
Mtb$^{R4\#}$	ILE 0.1	F80I	TTT→ATT	-	-
Mtb$^{R5\#}$	ILE 0.1	F80V	TTT→GTT	-	-
Mtb$^{R6\#}$	ILE 0.1	F80L	TTT→CTT	-	-
Mtb$^{R7\#}$	ILE 20	F80C	TTT→TGT	-	-
Mab$^{R1\#}$	ILE > 128 ILF > 128	-	-	P30H	CCC→CAC
Mab$^{R2\#}$	ILE 4 ILF > 128	F2L	TTC→TCC	-	-
Mab$^{R3\#}$	ILE 4 ILF > 128	M1-FERF-F2	Ins: TTCGAGAGATTC	-	-
Mab$^{R4\#}$	ILE 4 ILF > 128	Q17R	CAA→CGA	-	-
Mab$^{R5\#}$	ILE > 128 ILF > 128	H77D	CAC→GAC	-	-
Mab$^{R6\#}$	ILE > 128 ILF > 128	L88R	CTG→CGG	-	-
Mmr$^{R1\#}$	ILE 1 ILF 4	F2L	TTC→TCC	-	-
Mmr$^{R2\#}$	ILE 10 ILF 40	H77D	CAC→GAC	-	-
Mmr$^{R3\#}$	ILE 10 ILF 40	L88R	CTC→CGC	-	-
Msm^{R1*}	ILE 0.5 ILF 20	F2S	TTT→TCT	-	-
Msm^{R2*}	ILE 0.25 ILF 10	F2C	TTT→TGT	-	-
Msm^{R3*}	ILE 1 ILF 20	M1-L-F2	Ins: GTT	-	-
Msm^{R4*}	ILE 1 ILF 10	F5I	TTT→ATT	-	-
Msm^{R5*}	ILE 0.5 ILF 40	F80S	TTC→TCC	-	-
Msm^{R6*}	ILE 0.25 ILF 10	L88P	CTC→CCC	-	-

Msm^{R7*}	ILE 0.25 ILF 20	L88R	CTC→CGC	-	-
Msm^{R8*}	ILE 0.25 ILF 10	F2S; I197N	TTT→TCT; ATC→AAC	-	-

[#], Resistant mutants were selected from ILE-containing plates; [*], Resistant mutants were selected from ILF-containing plates; Ins, insertion; Underlines indicate mutated bases; - showed no mutation.

Molecular docking of ILE to the N-terminal domains (NTD) of MtbClpC1 and MtbClpX

Based on the reported structure of MtbClpC1-NTD[28] and the predicted structure of MtbClpX-NTD using AlphaFold2, we docked ILE to the MtbClpC1-NTD (Fig. 2a) and MtbClpX-NTD (Fig. 2b), respectively. The docking results indicate that the key residues involved in drug binding include the aforementioned mutation sites, namely Q17, H77, F80, and L88 in MtbClpC1-NTD, as well as P30 in MtbClpX-NTD. Given the structural similarity between ILE and ILF, and the observed cross-resistance, ILF likely binds ClpC1 and ClpX at similar binding sites.

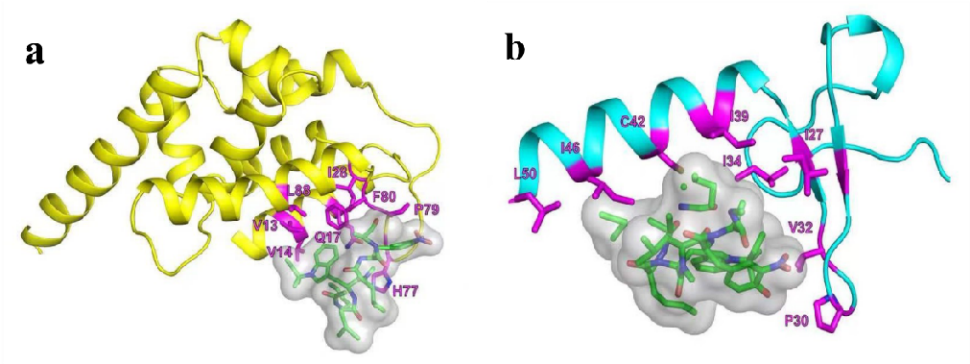

Fig. 2 | The graphical representation of crucial residues in the interaction between ILE and MtbClpC1-NTD as well as MtbClpX-NTD. a Crucial residues in the interaction between ILE and MtbClpC1-NTD. **b** Crucial residues in the interaction between ILE and MtbClpX-NTD. MtbClpC1-NTD, N-terminal domain of MtbClpC1 (residues 1–145); MtbClpX-NTD, N-terminal domain of MtbClpX (residues 1–112).

The effect of *clpC1* or *clpX* editng in Mab and Msm on their sensitivities to ILE/F

Given the slower growth rate and the absence of efficient genetic manipulation tools for Mtb compared to rapidly-growing mycobacteria such as Msm and Mab, we initially utilized these two NTM to validate the impact of ClpX or ClpC1 mutations

observed on ILE/F resistance. Utilizing CRISPR/Cpf1-mediated gene editing techniques[29,30], we introduced specific *clpC1* and *clpX* mutations into Mab and Msm, resulting in two Mab strains (wild-type ClpC1 ($ClpC1^{wt}$) to $ClpC1^{F2L}$; $ClpX^{wt}$ to $ClpX^{P30H}$) and two Msm strains ($ClpC1^{wt}$ to $ClpC1^{M1\text{-}L\text{-}F2}$; $ClpC1^{wt}$ to $ClpC1^{I197N}$). These genetically modified strains displayed varying levels of resistance as summarized in Table 3.

Notably, the $ClpX^{P30H}$ mutation in Mab conferred the highest resistance level, with MICs exceeding 128 μg mL^{-1} for both ILE and ILF. The $ClpC1^{F2L}$ mutation in Mab led to a more modest increase in resistance, elevating the MIC for ILE by eight times relative to the parent strain. The $ClpC1^{M1\text{-}L\text{-}F2}$ mutation in Msm increased the MICs of ILE/F by 4 and 6.4 times, respectively, compared to that of the parent strain. A comparative analysis of spontaneous mutants and gene-edited strains revealed that mutations at the F2 of ClpC1 in both Mab and Msm confer relatively low-level resistance to ILE/F, whereas the P30H mutation in Mab ClpX is associated with high-level resistance, underscoring its crucial role. It is noteworthy that the lack of impact of the Msm $ClpC1^{I197N}$ mutation on ILE and ILF resistance may be attributed to its location outside NTD (residues 1-145) of ClpC1, suggesting that resistance is primarily driven by alterations within the NTD. Furthermore, the spontaneous mutant strain harboring *clpC1*^{I197N} also possessed *clpC1*^{F2S} (Table 2), which may be the principal factor contributing to ILE/F resistance.

Table 3 | MICs of ILE and ILF against gene edited strains and corresponding spontaneous mutants

Strains	**Amino acid change**	**ILE MIC (μg mL^{-1})/ (fold change)**	**ILF MIC (μg mL^{-1})/ (fold change)**
Mab^{wt}	/	1	20
$Mab^{R2\#}$	$ClpC1^{wt}$ to $ClpC1^{F2L}$	4 / (4)	> 128 / (> 6)
Mab-$C1^{F2L}$	$ClpC1^{wt}$ to $ClpC1^{F2L}$	8 / (8)	> 128 / (> 6)
$Mab^{R1\#}$	$ClpX^{wt}$ to $ClpC1^{P30H}$	> 128 / (> 128)	> 128 / (> 6)
Mab-X^{P29H}	$ClpX^{wt}$ to $ClpC1^{P30H}$	> 128 / (> 128)	> 128 / (> 6)
Msm^{wt}	/	0.0625	2.5
Msm^{R3*}	$ClpC1^{wt}$ to $ClpC1^{M1\text{-}L\text{-}F2}$	1 / (16)	20 / (8)
Msm-$C1^{M1\text{-}L\text{-}F2}$	$ClpC1^{wt}$ to $ClpC1^{M1\text{-}L\text{-}F2}$	0.25 / (4)	16 / (6.4)

Msm^{R8*}	ClpC1^{wt} to ClpC1^{F2S} ClpC1^{wt} to ClpC1^{I197N}	0.25 / (4)	10 / (4)
Msm-C1^{I197N}	ClpC1^{wt} to ClpC1^{I197N}	0.0625 / (1)	2.5 / (1)

[#], Resistant mutants were selected from ILE-containing plates. [*], Resistant mutants were selected from ILF-containing plates. -C1 or -X means ClpC1 or ClpX was edited.

The sensitivity of Mab, Mmr or Msm overexpressing genes encoding subunit(s) of Clp proteases to ILE or ILF

The genes *clpX*^{wt} and *clpC1*^{wt}, along with their mutant variants, were inserted into two extrachromosomal plasmids, p60A or pMVA, each bearing distinct resistance markers (Supplementary Fig. 2). These genes were under the robust *hsp60* promoter to facilitate overexpression in autoluminescent strains of Mab (AlMab)[31], Msm (AlMsm)[32], and Mmr (AlMmr)[33]. Among these strains, only the AlMmr strain overexpressing ClpC1^{L88R} demonstrated resistance to both ILE/F when compared to the parent strain (Table 4). However, the overexpression of wild-type and mutated forms of ClpC1 or ClpX, as well as the concurrent overexpression of genes encoding the ClpC1P1P2 or ClpXP1P2 complexes in AlMab and AlMsm, did not alter their susceptibility to ILE or ILF. These findings are consistent with previous observations, suggesting that the overexpression of all mutated *clpC1* does not necessarily confer resistance to ClpC1-targeting compounds, and that efficacy varies across different mycobacterial species[34].

Table 4 | MICs of ILE and ILF against AlMmr strains overexpressing ClpC1 variants

Strains	ILE MIC (μg mL^{-1}) / (fold change)	ILF MIC (μg mL^{-1}) / (fold change)
AlMmr^{wt}	0.08	0.625
AlMmr::ClpC1^{wt}	0.08 / (1)	0.625 / (1)
AlMmr::ClpC1^{L88R}	0.625 / (8)	5 / (8)
AlMmr::ClpC1^{F2L}	0.08 / (1)	0.625 / (1)
AlMmr::ClpC1^{H77D}	0.08 / (1)	0.625 / (1)

The sensitivity of Mab or Msm strains, with either the *clpX* or *clpC1* gene knocked down, to ILE or ILF

The knockdown of *clpX* or *clpC1* in Mab (Fig. 3a) and Msm (Fig. 3b) strains resulted in heightened sensitivity to ILE/F. Upon induction with anhydrotetracycline (aTc) in the absence of ILE or ILF, growth inhibition was observed in both the *clpX* or

clpC1 knockdown strains of Msm and Mab, highlighting the crucial role of these proteins in cellular proliferation. This finding corroborates previous reports on their essentiality in Msm and Mab[35,36].

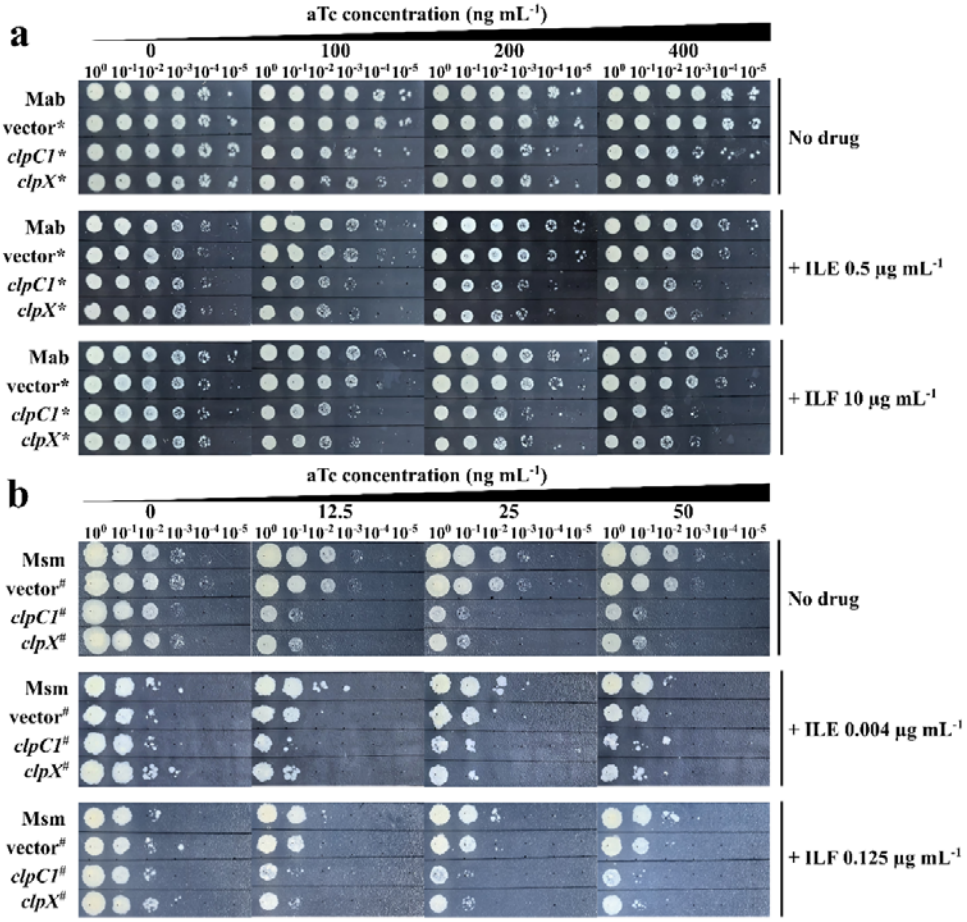

Fig. 3 | The impact of suppressing *clpX* or *clpC1* genes on the sensitivity of Mab and Msm to ILE or ILF. **a** The sensitivity of Mab to ILE or ILF upon gene suppression. **b** The sensitivity of Msm to ILE or ILF under similar conditions. aTc was served as the inducer for gene suppression. *, Mab strains contained varying plasmids: vector, a vector control with the empty plasmid pLJR962; *clpC1*, pLJR962-clpC1 for inducible inhibition of the *clpC1* gene; *clpX*, pLJR962-clpX for inducible inhibition of the *clpX* gene. #, Similarly, Msm strains were differentiated by the plasmids they harbored as that in Mab.

The interactions between ClpC1-NTD and either ILE or ILF, as well as the interactions between the ClpX-NTD and ILE

Since all mutations occurred within NTD of ClpC1 or ClpX across Mtb, Mab,

Msm, and Mmr, and their ClpC1-NTD or the first 64 amino acids of the ClpX-NTD (residues 1 – 112) sequences are identical (Supplementary Fig. 3 and 4), we specifically expressed and purified the NTDs of ClpC1 and ClpX from Mtb. Subsequently, the interactions between the MtbClpC1-NTD or MtbClpX-NTD with ILE or ILF were examined. We discovered that ILE increased the melting temperature (Tm) of MtbClpC1-NTD from 78.5□ to 81.5□ (Fig. 4a), signifying a significant enhancement in thermal stability (ΔTm of 3□). Conversely, ILF marginally augmented the thermal stability of the MtbClpC1-NTD by merely 1□ (Fig. 4b) compared to ILE. The stronger affinity of ILE over ILF correlates with its lower MIC. These findings suggest potential interactions of ILE/F with MtbClpC1-NTD. However, we could not discern any alteration in the melting temperature of MtbClpX-NTD by ILE/F. Nevertheless, it was evident that as the ILE concentration increased, less ClpX protein underwent degradation (Fig. 4c) in a drug affinity responsive target stability (DARTS) assay, which was employed to identify small molecule targets previously[17,37]. This implies that ILE can bind to the ClpX protein, shielding it from proteolytic digestion by pronase.

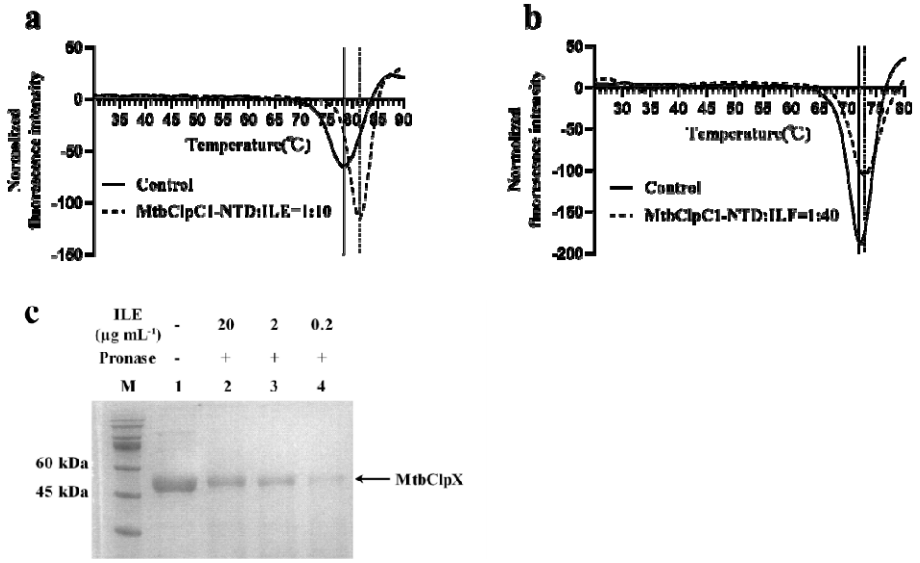

Fig. 4 | The interactions between ClpC1-NTD and either ILE or ILF, as well as the interactions between the ClpX and ILE. **a** The melting curves of MtbClpC1-NTD in the presence of ILE are shown. **b** The melting curves of MtbClpC1-NTD in the presence of ILF are

illustrated. Control, samples contained DMSO; Normalized fluorescence intensity refers to the fluorescence intensity normalized to the first time point after excitation for each well. **c** ILE protects wild-type MtbClpX from protease digestion, as analyzed by SDS-PAGE. Lanes: M, protein ladder; 1, MtbClpX without any treatment; 2 to 4, MtbClpX treated with different concentrations of ILE and digested by protease.

The impact of ILE on the proteolytic functions of the ClpC1P1P2 and ClpXP1P2 complexes, as well as its effect on the ATPase activities of ClpC1 and ClpX

Given the stronger interactions between MtbClpC1-NTD and ILE, we concentrated our efforts on evaluating ILE in subsequent biochemical assays. We discovered that ILE inhibited the proteolysis of the model substrate FITC-casein by $ClpC1^{wt}P1P2$ complex relative to the control group (Fig. 5a). However, the proteolytic activities of multiple mutant ClpC1P1P2 complexes remain unaffected at 10 μg mL^{-1} ILE compared to the control, with only partial inhibition noted at 20 μg mL^{-1} ILE (Fig. 5c-5f). ILE was found to be ineffective in altering the proteolytic activity of the ClpXP1P2 complex during the hydrolysis of GFP-ssrA (Fig. 5b). This may be attributed to the primary binding site for the ssrA tag being located in the AAA+ domain of ClpX rather than NTD, as demonstrated by *Escherichia coli* (*E. coli*) ClpXP, which can degrade GFP-ssrA even in the absence of its NTD[38]. Furthermore, the structure of the ClpXP·GFP-ssrA·SspB complex revealed that the adaptor SspB protein, tethered to the NTD of ClpX, positioned the C-terminal residues of the ssrA tag in the upper part of a closed axial channel of ClpX, closely resembling an adaptor-free recognition complex[39]. Nonetheless, based on the mutation location within the *clpX* gene and docking results, we hypothesize that ILE primarily binds to the NTD of ClpX, potentially not preventing ssrA-tagged substrates from entering the axial channel of ClpX.

We observed that ILE did not impact the ATP-dependent enzymatic activities of ClpC1 and ClpX, as no significant differences in ATPase activities were detected across varying ILE concentrations compared to controls (Supplementary Fig. 5).

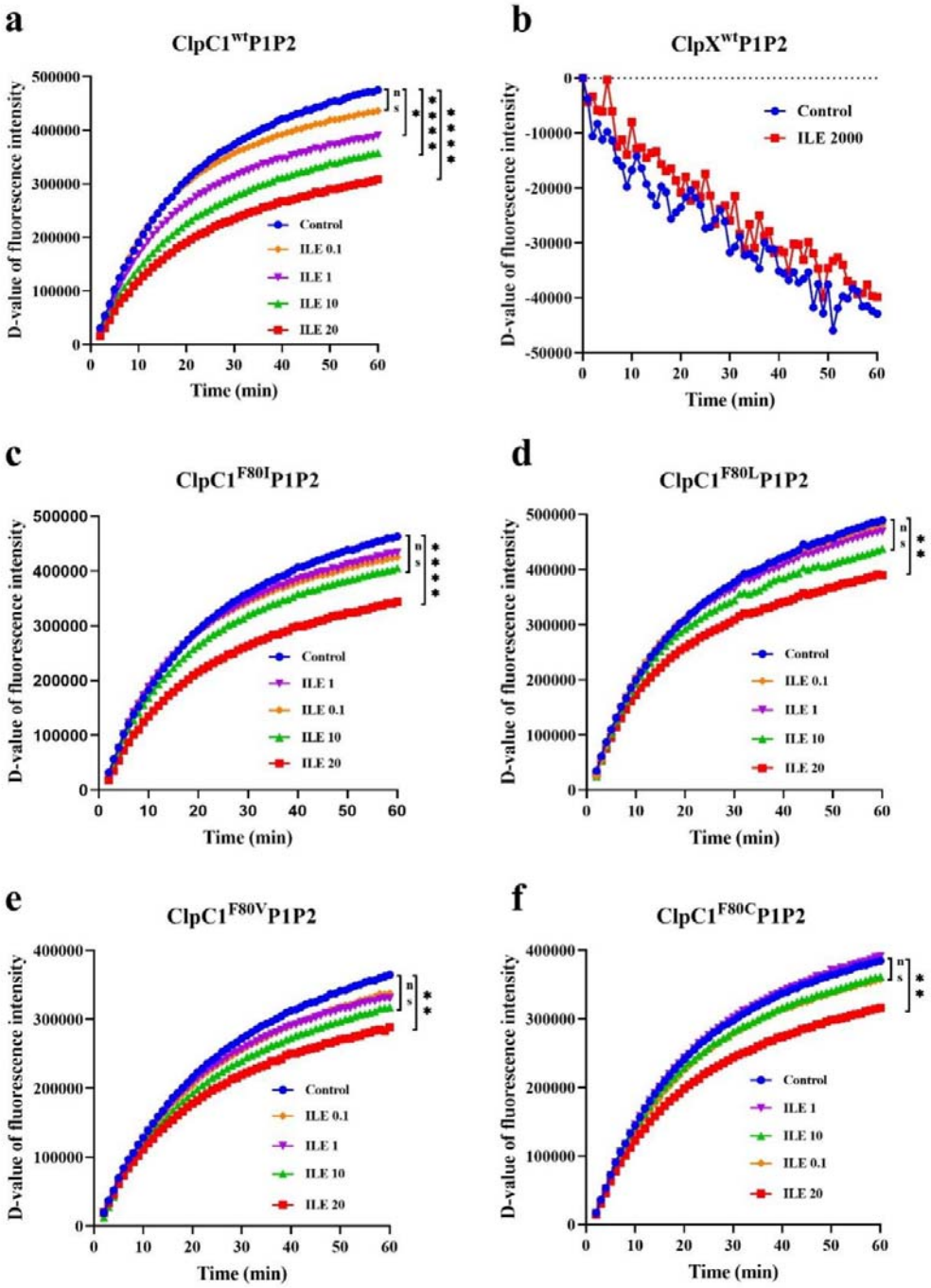

Fig. 5 | The proteolytic activities of the ClpC1P1P2 and ClpXP1P2 complexes in response to ILE treatment. a, **c-f** The proteolytic activities of various ClpC1P1P2 complexes in response to ILE treatment. **b** The proteolytic activities of the ClpXP1P2 complexes after ILE treatment. The formation of complexes was as follows: ClpC1^{wt}P1P2, ClpC1^{F80I}P1P2, ClpC1^{F80L}P1P2, ClpC^{1F80V}P1P2, and ClpC1^{F80C}P1P2 represent the assembly of wild-type and mutant ClpC1 with

ClpP1 and ClpP2. The ClpXP1P2 complex is formed by the association of wild-type ClpX with ClpP1 and ClpP2. $^{*}P < 0.05$; $^{**}P < 0.001$; $^{****}P < 0.00001$; and ns, no significant difference, where $P > 0.05$. Numbers following the drug names indicate the working concentrations (μg mL^{-1}). The D-value of fluorescence intensity represents the change in fluorescence intensity by subtracting the initial fluorescence intensity from the fluorescence intensity of subsequent detections.

The effect of ILE/F treatment on the morphology of Msm cells

To elucidate the bactericidal mechanisms of ILE/F, Msm was cultured with 0.125 μg mL^{-1} of ILE or 5 μg mL^{-1} of ILF for 15 hours. Notably, the cell lengths of Msm increased from 2.07 ± 0.48 μm to 5.95 ± 2.16 μm and 9.41 ± 2.40 μm following treatment with ILE and ILF, respectively (Fig. 6). In comparison to untreated Msm, ILE/F both induced a marked increase in cell length and a pronounced inhibition of cell division, as evidenced by the formation of division septa (Fig. 6b and Fig. 6c). This observation is consistent with the phenotype observed in Msm upon *clpX* gene silencing[36], and the established role of ClpX in regulating FtsZ assembly and Z-ring formation which are crucial processes for cell division in Mtb[40].

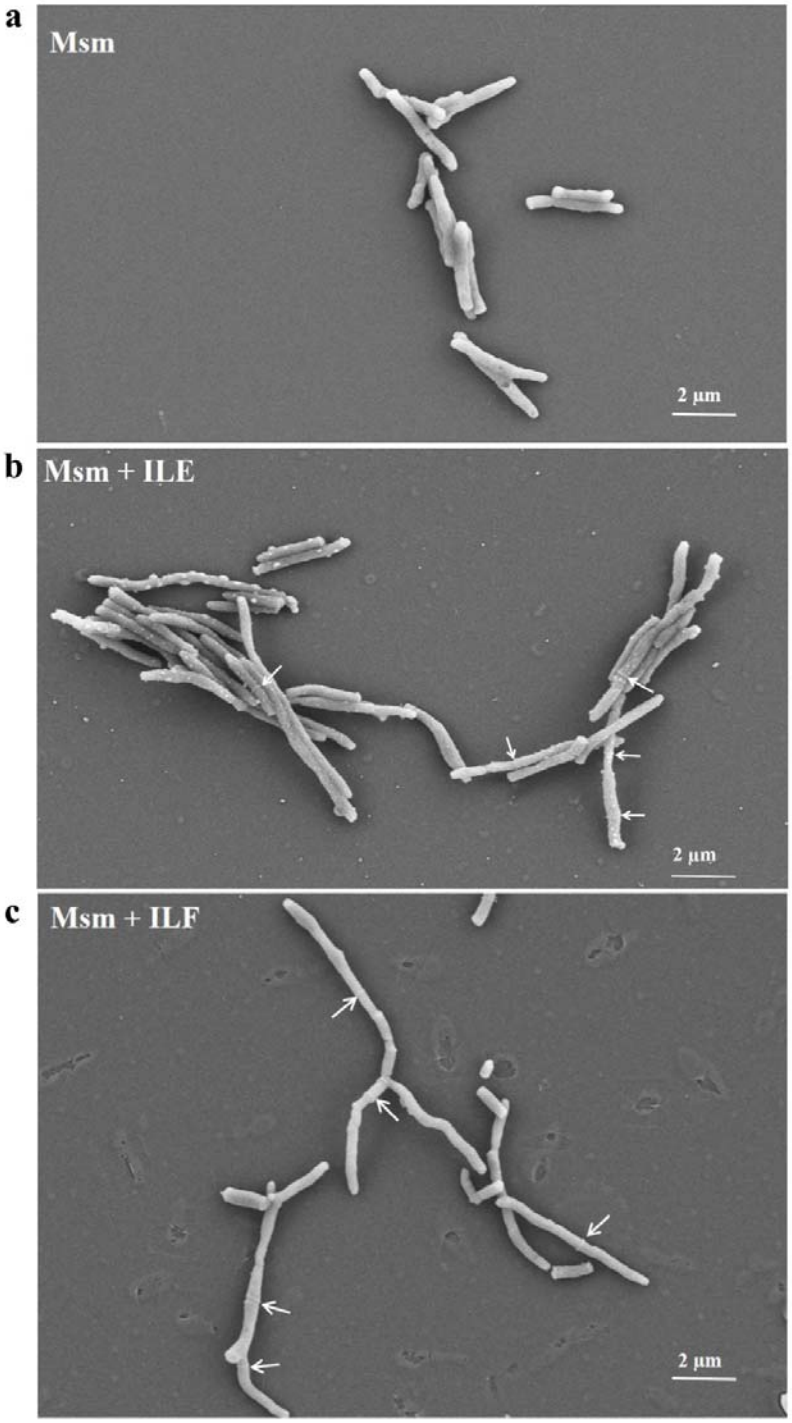

Fig 6 | The cell morphology of Msm strains before or after treatment with ILE or ILF. a The cell morphology prior to any treatment. **b** The cell morphology of Msm treated with a concentration of 0.125 μg mL^{-1} ILE. **c** The cell morphology of Msm treated with a concentration of 5 μg mL^{-1} ILF. The white arrows highlight the division septa.

Proteomic signature of the cells treated with ILE

The proteomics of cells treated with ILE was investigated to elucidate the adaptive responses of Mtb during ILE treatment, thereby enhancing our understanding of its activity and MOA. A differential expression of proteins was noted post-treatment with ILE (Supplementary Table 1 for details). In comparison to non-treated cells, Mtb cells subjected to ILE exhibited an upregulation of proteins associated with protein synthesis, including various 50S and 30S ribosomal proteins such as RpsG, RpsS, RpmB, and RpmF. However, only RplR and RpsC displayed downregulation. Key sigma transcription factors, which are essential for gene transcription, namely SigE, SigB, and SigL, were also upregulated. Notably, components of the toxin-antitoxin system, including toxin factors Rv0240 and Rv2142c, as well as antitoxins Rv0660c and Rv0748, were upregulated in response to ILE treatment. Conversely, no down-regulated components of either toxins or antitoxins were observed. This finding is consistent with previous reports suggesting that certain toxin-antitoxin proteins are targeted by the ClpXP1P2 complex[9]. Surprisingly, ClpX was found to be downregulated, potentially leading to an accumulation of toxin-antitoxin proteins and contributing to the altered cell morphology in ILE-treated Mtb[9].

The expression of membrane proteins was significantly perturbed, with some experiencing increased expression while others showed a decrease. Proteins involved in the intermediary metabolism and respiration of Mtb, such as QcrA, QcrC, and CydD, were downregulated, indicating a potential impact of ILE on respiratory pathways. Changes in lipid metabolism-related proteins were also evident, including the upregulation of FadE9, FadE29, and FadD24, alongside the downregulation of FadD9, FadE6, FadE12, and FadE24. Furthermore, numerous membrane proteins (e.g., MmpL2, EccD5, EccE2) exhibited significant alterations in expression, whereas others like MmpS3, SecF, and TatA were downregulated in the presence of ILE.

Discussion

The study of natural cyclic peptides has emerged as a focal point in the current research on drugs against Mtb. In comparison to the reported cycloheptapeptides, ILE demonstrates superior anti-Mtb activity. Specifically, rufomycin I inhibited Mtb growth at a MIC of 60 nM by day 14 when tested with the autoluminescent Mtb strain[19], while ILE achieves an MIC of 48 nM (equivalent to 0.05 μg mL^{-1}) by day 15 (Fig. 1a). Moreover, the MIC of ILE is more than twice as low as those of cyclomarin A (100 nM)[13], ecumicin (160 nM)[13], and lassomycin (410 nM)[13], which were reported elsewhere. While these compounds exhibit activity against a range of NTM, only rufomycin I and ILE exhibit efficacy against Mab[15], indicating their potential as therapeutic agents for diseases caused by Mab.

Previously, the combination effects of cycloheptapeptides with anti-TB drugs had not been explored, leaving their potential as adjuvants to current TB therapies unresolved[14-17]. Notably, our findings on combinatorial activity suggest that ILE/F have the potential to enhance the efficacy of existing anti-TB drugs, including INH, EMB, CLF, BDQ, and TB47. Proteomic analysis indicated that ILE modulated the expression of four proteins (SigL, Ndh, FadE24, and Glf) associated with metabolic pathways affected by INH. Specifically, SigL and Ndh were significantly upregulated, whereas FadE24 and Glf were downregulated. SigL has been reported to regulate the expression of KatG, which is crucial for the activation of INH[41,42], and Ndh has been identified to influence the NADH/NAD+ ratio, affecting INH-NAD formation[43]. INH-resistant Mtb has been found to carry mutations in FadE24[44]. Upregulation of Glf was hypothesized to contribute to INH resistance in Mtb either by binding to a modified form of INH or by sequestering a factor such as NAD^+ required for INH activity[45]. Additionally, key proteins in the electron transport chain of Mtb, such as QcrA, QcrC, and CydD, were all downregulated after treatment with ILE. The QcrB protein is the target of the TB47[33,46]. Furthermore, given the interchangeability of the two electron transfer chains, it was previously speculated that the inhibitory effect of the QcrB

inhibitor TB47 on Mtb would be enhanced when the Cyt-bds complex containing CydD is inhibited[33].

Although ILE and ILF have demonstrated potent activity against Mtb, their MOAs remained elusive[18]. Previous studies had identified cyclic peptides that specifically target ClpC1[28]. WGS and Sanger sequencing of spontaneous mutants resistant to ILE or ILF also identified ClpC1 as the primary target in Mtb, Mab, Msm, and Mmr. The mutations in ClpC1 found in ILE- or ILF-resistant mutants were similar to those reported in mutants resistant to known ClpC1-targeting cyclic peptides, with the exception of unique insertion mutations discovered between M1 and F2 in both Mab and Msm[14,15,17,34]. Prior research had primarily relied on indirect genetic validation of these mutations through overexpression[34]. With advancements in genetic manipulation tools for mycobacteria, we have directly confirmed the role of specific mutations, such as the F2L mutation in Mab and the newly discovered insertion mutation in Msm, in conferring resistance to ILE and ILF through gene editing for the first time.

Interestingly, no ClpX mutations had been reported in mutants resistant to these compounds[14,15,17]. However, our findings indicate that ILE-resistant mutants harboring ClpX mutations also exhibit cross-resistance to ILF, suggesting that these two components of ilamycins may interact with multiple targets within the mycobacterial proteolytic machinery. This interaction could explain the superior activity of ILE against Mtb compared to previously reported compounds. Furthermore, we have directly confirmed that ClpX mutations can lead to high-level resistance to both ILE and ILF through gene editing. These observations suggest that certain cyclic peptide natural products, such as rufomycin I, may also target the ClpX protein. The selection of rufomycin I- and ecumicin-resistant mutants through stepwise inoculation on plates impregnated with increasing concentrations of compounds may have overlooked strains with high levels of resistance that acquired the ClpX mutation[15,17]. Similarly, for lassomycin, only a limited number of resistant mutants with relatively low levels of resistance were obtained, potentially hindering the discovery of another target, ClpX[14]. In the case of cyclomarin A, the target was identified using affinity

chromatography and chemical proteomics. However, our results from DSF experiments suggest that ClpX protein may not have been isolated during the identification of cyclomarin A's targets due to its weaker affinity with ClpX. This study marks the first time that ClpX has been identified as a target for discovering anti-Mtb drugs, paving the way for novel strategies in anti-mycobacterial drug development.

The MOA of ILE differs from ecumicin and lassomycin, which stimulate ClpC1 ATPase activity but hinder substrate degradation, as well as cyclomarin A, which activates both ATPase and proteolytic functions[14,17,34]. Notably, ILE does not influence the ATPase activities of ClpX and ClpC1. However, ILE inhibits the proteolytic activity of the ClpC1P1P2 complex, mirroring the MOA of rufomycin I [15]. Prior investigations have not reported that these cyclic peptide compounds, particularly rufomycin I, could target the ClpX protein to affect the activity of the ClpXP1P1 complex[14,15,17,34]. In this study, ILE exhibited no significant effect on the ATPase activity of ClpX, consistent with previous findings that showed no substantial changes in ATPase activity after NTD deletion in Mtb ClpX[47]. MtbClpX-NTD has been reported to play a vital role in substrate recognition and binding within the ClpX protein[47]. They also discovered that the aliphatic residue in the third-to-last position of the ssrA tag substantially impacts the binding affinity of Mtb ClpX and the residence time of substrate proteins on Mtb ClpX[47]. Nevertheless, the primary binding site for the ssrA tag may reside within the AAA+ domain of Mtb ClpX rather than NTD, similar to *E. coli* ClpXP, which can degrade GFP-ssrA even in the absence of its NTD[38]. This observation could explain why ILE does not affect the activity of the ClpXP1P2 complex in degrading GFP-ssrA. These insights emphasize the need for future studies to utilize ssrA variant-tagged substrates or other suitable substrates to clarify the effect of ILE on the proteolytic activity of the ClpXP1P2 complex.

In summary, the potent and broad antimycobacterial activities of ILE/F underscore their potential for further development as effective agents against mycobacteria, especially drug-resistant strains. The cumulative evidence from this and related studies[14,15,17,34] identify ClpC1P1P2 and, more importantly, ClpXP1P2 as

promising targets for the development of antimycobacterial agents. A dual-targeting strategy that affects both simultaneously is a rational approach.

Methods

Bacterial strains and media

Bacterial strains used in this study are listed in Supplementary Table 2. Mtb, Mmr, Mab, and Msm were grown in Middlebrook 7H9 broth supplemented with OADC (comprising 0.005% oleic acid, 0.5% bovine serum albumin, 0.2% dextrose, 0.085% catalase). Mab GZ002 [48] and Msm mc^2155 were used as the wild-type strains. *E. coli*, *Enterococcus faecium*, *Staphylococcus aureus*, *Acinetobacter baumannii*, *Klebsiella pneumoniae* and *Pseudomonas aeruginosa*, cells were grown in Luria-Bertani (LB) broth.

MICs to mycobacteria determination

The MICs of ILE and ILF were determined using a cost-effective *in vitro* assay as previously described against a selectable marker-free autoluminescent Mtb $H_{37}Ra$ (AlRa), AlRv, AlMab, AlMsm and AlMmr[31-33,49]. The MIC_{lux} was defined as the lowest concentration that could inhibit > 90% relative light units (RLUs) compared with that from the untreated controls[31-33,49]. The MICs of the ILE were also determined by a well-established microplate alamar blue assay (MABA) against Mtb $H_{37}Ra$, $H_{37}Rv$ and nine clinical Mtb strains isolated from pulmonary TB patients hospitalized at Guangzhou Chest Hospital, Guangzhou, China[20,31]. The MIC, as determined by the MABA method, is defined as the lowest concentration that prevents the color change from blue to pink, as observed with the naked eye.

MICs to non-mycobacteria determination

The MICs of ILE or ILF against *Enterococcus faecium*, *Staphylococcus aureus*, *Acinetobacter baumannii*, *Klebsiella pneumoniae* and *Pseudomonas aeruginosa* were determined by observing the turbidity after 16 h of incubation in LB broth at 37□. The MIC was defined as the lowest concentration, resulting in clarity in turbidity relative to that of untreated control cultures[50,51].

Combined activity of ILE or ILF with other compounds *in vitro*

The combined activity of ILE or ILF with other compounds, such as INH, RIF,

EMB, STR and TB47, was evaluated in vitro using the checkerboard method. The fractional inhibitory concentration index (FICI) was interpreted as follows: synergistic (FICI of ≤ 0.5), partially synergistic (0.5 < FICI < 1.0), additive (FICI = 1.0), indifferent (1.0 < FICI ≤ 4.0), and antagonistic (FICI > 4.0)[52,53].

Activity in macrophage culture

The growth inhibition of AlRv in macrophage culture was assessed as previously described[52]. The cell density of mouse macrophages RAW264.7 was adjusted to 5×10^5 cells mL^{-1}. 100 μL of cells per well were added to 96-well plates and cultured overnight for adherence. The AlRv concentration was adjusted to 3×10^6 RLU mL^{-1}, and 100 μL of AlRv was added to each well. The plates were then incubated at 37□ for 6 h. The cells were washed three times with DMEM to remove non-phagocytosed AlRv and treated with DMEM containing amikacin (100□μg mL^{-1}) for 2□h to eliminate the extracellular bacteria. The cells were washed twice with DMEM to remove residual amikacin. A total of 195 μL of DMEM containing 10% fetal bovine serum and 5 μL of the two-fold dilutions of various ILE concentrations were added to the cells. The mixture was incubated at 37□ with 5% CO_2, and the RLUs were measured on days 1-5 or 7 of incubation. RIF (1 μg mL^{-1}) and dimethyl sulfoxide (DMSO) were used as positive and negative controls, respectively.

ILE or ILF-resistant mutants

Broth cultures of AlRa, AlRv, AlMab, and AlMmr, having OD_{600} 0.6-1.3, were plated on 7H11 plates containing ILE at 0.1, 0.5, 2.5, 5, 10 or 20 μg mL^{-1}. Broth cultures of AlMsm (OD_{600} 0.6-1.3) were plated on 7H11 plates containing ILF at 10, 20 or 40 μg mL^{-1}. The bacterial colonies grown on the ILE- or ILF-containing plates were selected and grown in liquid culture for drug susceptibility testing to confirm the drug resistance phenotype.

WGS analysis

WGS analysis was conducted on the parent strains of Mtb, Mab, and a subset of the confirmed ILE-resistant mutants. The sequencing was performed by the Beijing Genomics Institute in China. Subsequently, the obtained reads were aligned with the

reference genome sequence and compared to that of the parent strain. Mutations identified through WGS in the drug-resistant mutants were validated by amplifying and sequencing the *clpX* and *clpC1* genes using Sanger sequencing. Additionally, the *clpX* and *clpC1* genes from other ILE- or ILF-resistant mutants, including Mtb, Mab, Msm, and Mmr, were amplified and sequenced using Sanger sequencing (primer sequences are provided in Supplementary Table 3).

Molecular docking analysis

To evaluate the binding affinities and interaction modes among ILE, MtbClpC1-NTD, and MtbClpX-NTD, we employed Autodock Vina 1.2.2, a computational protein-ligand docking software as referenced in study[54]. The structure of ILE was obtained from PubChem Compound[55]. The 3D coordinates of MtbClpC1-NTD were retrieved from the Protein Data Bank (PDB) with PDB code 6CN8 and a resolution of 1.4 Å, while the structure of MtbClpX-NTD was predicted using AlphaFold2.

For the docking analysis, all protein and ligand files were converted to the PDBQT format; water molecules were excluded, and polar hydrogen atoms were supplemented. A grid box was positioned to envelop the domain of each protein, facilitating unrestricted molecular movement. The dimensions of the grid box were set to 30 Å × 30 Å × 30 Å, with a grid point spacing of 0.05 nm. The molecular docking experiments were executed using Autodock Vina 1.2.2, which is accessible at http://autodock.scripps.edu/.

Overexpression of *clpX* or *clpC1* in Mab, Mmr or Msm

clpC1^{wt}, *clpC1*^{mt} (mutated *clpC1*), *clpX*^{wt} and *clpX*^{mt} from Mtb, Mab, Mmr and Msm were amplified using primers detailed in Supplementary Table 3 and subsequently cloned into the plasmid p60A or pMVA with multi-copy under the control of the *hsp60* promoter as depicted in Supplemantary Fig. 2[33]. The plasmids were then transformed into AlMab, AlMmr, and AlMsm. Additionally, the *clpP1*, *clpP2* and *clpX* or *clpC1* of Mab were amplified from the genome of Mab^{wt} and inserted into the plasmid pMVA under the control of the *hsp70* or *hsp60* promoters to enable the simultaneous expression of ClpXP1P2 or ClpC1P1P2. The MICs of the

recombinant strains to ILE or ILF were determined using the aforementioned protocols.

Silencing *clpX* or *clpC1* genes in Mab or Msm

The CRISPR-Cas9 system was employed for targeted gene silencing of *clpX* and *clpC1* as described in reference[56]. Small guide RNAs (sgRNAs) of 20 base pairs were designed to target the coding regions of *clpX* and *clpC1* on their sense strands. The oligonucleotides were annealed and then ligated with linearized pLJR962[56]. Plasmids harboring sgRNAs against *clpX* or *clpC1*, along with the empty vector pLJR962[56] as a control, were introduced into Mab and Msm cells via electroporation (Supplementary Table 4). The gene-silenced strains and the control strain carrying the empty vector were cultured, and the efficacy of gene silencing was assessed. 4 μL of ILE were added to each well of the 96-well microplate, resulting in a final concentration gradient ranging from 8 to 0.0313 μg mL^{-1}. Bacterial cultures were adjusted to an OD_{600} of approximately 0.5 and then diluted 1000-fold in 7H9 medium, with or without aTc.

The diluted bacteria were then divided into the experimental group (+ aTc 50 ng mL^{-1}) and the control group (- aTc). 196 μL of these two groups were then inoculated into the 96-well microplate separately. The microplates were incubated at 37°C for 3 days. The MIC was defined as the lowest concentration that prevented visible bacterial growth. All experiments were conducted in triplicate and repeated independently at least twice.

Tenfold serial dilutions of Mab^{wt} or Msm^{wt}, the control strain carrying the empty vector, and the gene-silenced strains were prepared after reaching an OD_{600} of approximately 0.9. For Mab, 1 μL of each dilution was spotted on plates containing either 0.25, 0.5, and 1 μg mL^{-1} ILE or 5, 10, and 20 μg mL^{-1} ILF with varying concentrations of aTc (0, 100, 200 and 400 ng mL^{-1}). For Msm, 1 μL of each dilution was spotted on plates containing either 0.004, 0.008, and 0.01625 μg mL^{-1} ILE or 0.125, 0.25, and 0.5 μg mL^{-1} ILF with varying concentrations of aTc (0, 12.5, 25 and 50 ng mL^{-1}). Control plates received 1 μL of each dilution with aTc alone. The plates

were incubated at 37□ for 3 days. The experiment was performed in triplicate and repeated twice.

CRISPR/Cpf1-mediated gene editing of *clpX* and *clpC1* genes in Mab and Msm

The CRISPR/Cpf1-associated recombination have been previously employed for gene editing in both Mab and Msm recently[29,30]. Initially, the pJV53-Cpf1 plasmid was electroporated into Mab^{wt} and Msm^{wt} strains, resulting in the Mab::pJV53-Cpf1 and Msm::pJV53-Cpf1, respectively. Subsequently, crRNAs were designed to target specific 25 nucleotide sequences adjacent to the 5'-YTN-3' motif on the template strand of the target genes (Supplementary Table 4). Oligonucleotides for crRNA expression were ligated into the pCR-zeo vector. These constructed vectors were then electroporated into the respective acetamide-induced cells of Mab::pJV53-Cpf1 or Msm::pJV53-Cpf1. For the induction of Cpf1 expression, aTc was added to 7H11 agar plates to achieve a final concentration of 200 ng mL^{-1}. These plates were cultured at 30□ for 3-5 days. Individual colony was picked and screened to confirm successful editing at the target gene site via PCR and Sanger sequencing (primers listed in Supplementary Table 3). The MICs of the edited strains to ILE and ILF were determined using the methods described earlier.

Expression and Purification of Proteins

The Mtb ClpP1 (residues 7-200) and ClpP2 (residues 13-214) with N-terminal His_6-SUMO tags were expressed and purified. Briefly, ClpP1 and ClpP2 were overexpressed individually in *E. coli* BL21 (λDE3) in LB broth at 16□, following induction with 0.5 mM isopropyl β-D-1-thiogalactopyranoside (IPTG) for approximately 16 h. Cells were resuspended and lysed; The His-tagged ClpP1/ClpP2 proteins were subsequently purified via nickel affinity chromatography and eluted with the same buffer supplemented with 250 mM imidazole. The His_6-SUMO tag of eluted proteins was removed by ubiquitin-like-protease 1 at 4□. After purifying the tag-free proteins, peak fractions were collected and concentrated through anion exchange chromatography. These fractions were then applied to Superdex 200 16/600 (GE Healthcare) for final purification. ClpP1 and ClpP2 were then concentrated in

amicon centrifugal concentration devices to a tetradecamer concentration of more than 80 μM.

clpX^{wt} and *clpX*^{P30H} were inserted into the pGEX-6P-1 vector, which had a His_6-tag at the C-terminal and an HRV 3C protease cleavage site. After induction for 18 h at 16□, the cells were collected by centrifugation. The pellet was then resuspended and lysed. After centrifugation, the supernatant was loaded onto a GST column and eluted. The eluent underwent digestion at 4□ for 26 h with enough HRV 3C protease. The fractions containing the target protein were then pooled, concentrated to 1 mL, and purified with a SuperoseTM 6 increase 10/300 GL column.

clpC1^{wt}, its mutants (F80I/V/L/C), and *gfp*-ssrA (AGKEKQNLAFAA) were inserted into the pET-28a vector that had an N-terminal His_6-tag. The recombinant strains were cultured in LB broth at 37□ until the OD_{600} reached 0.6-0.8. After 18 h of induction with 0.5 mM IPTG at 18□, the pellet was suspended and lysed. Following the loading of the supernatant onto a Ni-NTA column, the proteins were washed and then eluted. The fractions were then pooled and loaded onto a SuperoseTM 6 increase 10/300 GL column.

The coding gene sequence of MtbClpC1-NTD and MtbClpX-NTD were inserted into the pET-28a vector with a C-terminal His_6-tag and an HRV 3C protease cleavage site. The expression and purification methods of MtbClpC1-NTD and MtbClpX-NTD were consistent with the methods described above.

DSF

The binding of ILE or ILF to the MtbClpC1-NTD and MtbClpX-NTD was detected using DSF, following established protocols[57,58]. A 5 μM solution of either MtbClpX-NTD or MtbClpC1-NTD was incubated with varying concentrations of ILE or ILF (ranging from 12.5 to 400 μM), as well as DMSO for 30 minutes, subsequently mixed with Sypro Orange fluorescent dye. Fluorescence measurements were recorded using the CFX96 Real-Time System (Bio-rad), which involved heating 8-tube PCR Strips from 25□ to 95□ at a constant rate of 0.4□ min^{-1}. The excitation and emission filters were adjusted to wavelengths of 460 nm and 510 nm, respectively. Data

collection was facilitated by the CFX Manager software, with analysis performed using GraphPad Prism version 8.3.0. To ensure accuracy, all measurements were performed in triplicate.

DARTS

DARTS was employed to detect the binding between ILE and Mtb ClpX, following well-established protocols[17,37]. The ClpX concentration was determined using a BCA protein assay kit and adjusted to a total protein concentration of 0.5 mg ml^{-1} with 1 × TNC buffer (50 mM Tris-Cl pH 8.0, 50 mM NaCl, and 10 mM $CaCl_2$) for DARTS application. ClpX was divided into 19 μL aliquots and incubated with DMSO (as a control) or treated with ILE at final concentrations of 0.2, 2, and 20 μg ml^{-1} for 60 minutes at room temperature. Pronase (2 μL at 2.5 μg ml^{-1}) was then added to each ILE-treated sample, while 2 μL TNC buffer was added to each control sample, and incubation continued for an additional hour at room temperature. Subsequently, 5 μL of 5×SDS-PAGE loading buffer was added to the digested samples, and the mixtures were heated at 95□ for 10 min to terminate the digestion reaction. The sample proteins were then separated on 12% SDS-PAGE gels, stained with SimplyBlue SafeStain, and finally subjected to decolorization and photography.

Proteolytic activity assay of ClpC1P1P2 and ClpXP1P2

The proteolytic activity of ClpC1P1P2 and ClpXP1P2 were measured at 37□ in white 96-well plates using a Multimode Plate Reader. ILE was added at final concentrations of 0, 0.1, 1, 10, and 20 μg mL^{-1} in each well of a white 96-well plate. A 100 μL reaction mixture was formulated with either 2 μM ClpP1P2, 1 μM ClpC1 or ClpX, and 2.5 μM fluorescein isothiocyanate (FITC)-casein for ClpC1P1P2 or 2 μM GFP-SsrA for ClpXP1P2. The hydrolysis of FITC-casein and GFP-SsrA was continuously monitored at 535 nm (with excitation at 485 nm). Measurements were performed in triplicate.

ClpC1 and ClpX ATPase activities assay

The ATPase activities of Mtb ClpC1 and ClpX were assessed using a free-phosphate detection assay with the Biomol Green reagent. To each well of a

transparent 96-well plate, 5 μL of various concentrations of ILE (0, 0.08, 0.16, 0.31, 0.625, 1.25, 2.5, 5 and 10 μg mL^{-1}) was added. Subsequently, either ClpX or ClpC1 was diluted to a concentration of 0.1 μg mL^{-1} in the reaction mixture. 90 μL ClpC1 and ClpX were then added to a 96-well plate and incubated at 37□ for 1 h. The reaction was initiated by adding 5 μL of 1 mM ATP to the reaction mixture, which was maintained at 37□ for an additional hour. The final volume of the reaction mixture was adjusted to 100 μL. Post reaction, 100 μL of Biomol Green reagent was introduced to determine the amount of free phosphate. After a 30-minute incubation at room temperature, the resulting reaction product was measured at 620 nm using a Multimode Plate Reader. The concentration of free phosphate liberated from ATP by ClpX and ClpC1 was calculated using a standard curve based on the known concentration of free phosphate. Measurements were performed in triplicate.

Microscopy of ILE- or ILF-treated Msm

Treatment of exponentially growing Msm was conducted using 0.125 μg mL^{-1} ILE or 5 μg mL^{-1} ILF for a duration of 15 hours. The bacteria were immobilized with a 4% glutaraldehyde solution, followed by three washes and resuspension in phosphate-buffered saline (PBS). Bacterial suspensions were then applied to 5 mm cell slides, which were placed in a 24-well plate to dry naturally. Afterward, the cell slides underwent three additional PBS washes. The cell slides were subsequently soaked in ascending concentrations of ethanol solutions (70%, 80%, 90%, 100%) for 10 minutes each. Finally, the cell slides were dried using the critical point drying method and coated with an electrically-conducting material. Observations of bacterial morphology were made using a GeminiSEM 300 ultra-high resolution field emission cryo-scanning electron microscope.

Proteomic analysis

The AlRa cells were treated with 0.0125 μg mL^{-1} of ILE for 5 days in triplicate for 4D label-free phosphoproteomic analysis. To maintain comparable cell density between the untreated and ILE-treated groups, the untreated cells were diluted on the same day as the compound addition, prior to sample collection. The cells were

resuspended and boiled for 20 min. Subsequently, the samples were sent to APTBIO (Shanghai, China) for proteomic testing and analysis.

To compare the abundance of phosphopeptides between the control and treatment samples, label-free quantification was performed with a minimum fold change of 1.5 to determine the differentially expressed phosphopeptides. Additionally, the student's *t*-test was employed to detect significant differences between the control and treatment samples,with $P < 0.05$ indicating significance. Functional category analysis was performed using Mycobrowser (https://mycobrowser.epfl.ch/). Protein functional annotation was conducted with DAVID (https://david.ncifcrf.gov/summary.jsp), and differentially expressed proteins were listed in Supplementary Table 1.

Statistical analysis

Statistical analysis was conducted using GraphPad Prism 8.3.0. The unpaired *t*-test was applied to ascertain statistical significance, with $P < 0.05$ deemed significant.

References

1. Miotto P, Zhang Y, Cirillo DM, Yam WC. Drug resistance mechanisms and drug susceptibility testing for tuberculosis. *Respirology* **23**, 1098-1113 (2018).
2. Pfyffer G. Drug-resistant tuberculosis: resistance mechanisms and rapid susceptibility testing. *Schweiz Med Wochenschr* **130**, 1909-1913 (2000).
3. Fedrizzi T, *et al*. Genomic characterization of nontuberculous mycobacteria. *Sci Rep* **7**, 45258 (2017).
4. Wu M-L, Aziz DB, Dartois V, Dick T. NTM drug discovery: status, gaps and the way forward. *Drug Discov Today* **23**, 1502-1519 (2018).
5. Fraga H, *et al.* Development of high throughput screening methods for inhibitors of ClpC1P1P2 from Mycobacteria tuberculosis. *Anal Biochem* **567**, 30-37 (2019).
6. Lupoli TJ, Vaubourgeix J, Burns-Huang K, Gold B. Targeting the proteostasis network for mycobacterial drug discovery. *ACS Infect Dis* **4**, 478-498 (2018).
7. Lee H, Suh JW. Anti-tuberculosis lead molecules from natural products targeting Mycobacterium tuberculosis ClpC1. *J Ind Microbiol Biotechnol* **43**, 205-212 (2016).
8. d'Andrea FB, Poulton NC, Froom R, Tam K, Campbell EA, Rock JM. The essential *M. tuberculosis* Clp protease is functionally asymmetric *in vivo*. *Sci Adv* **8**, eabn7943 (2022).
9. Texier P, *et al.* ClpXP-mediated degradation of the TAC antitoxin is neutralized by the SecB-like chaperone in *Mycobacterium tuberculosis*. *J Mol Biol* **433**, 166815 (2021).
10. Raju RM, *et al*. *Mycobacterium tuberculosis* ClpP1 and ClpP2 function together in protein degradation and are required for viability *in vitro* and during infection. *PLoS pathogens* **8**, e1002511 (2012).
11. Akopian T, Kandror O, Raju RM, UnniKrishnan M, Rubin EJ, Goldberg AL. The active ClpP protease from *M. tuberculosis* is a complex composed of a heptameric ClpP1 and a ClpP2 ring. *EMBO J* **31**, 1529-1541 (2012).
12. Sassetti CM, Boyd DH, Rubin EJ. Genes required for mycobacterial growth

defined by high density mutagenesis. *Mol Microbiol* **48**, 77-84 (2003).

13. Boshoff HI, Malhotra N, Barry III CE, Oh S. The antitubercular activities of natural products with fused-nitrogen-containing heterocycles. *Pharmaceuticals (Basel)* **17**, 211 (2024).
14. Gavrish E, *et al*. Lassomycin, a ribosomally synthesized cyclic peptide, kills *Mycobacterium tuberculosis* by targeting the ATP-dependent protease ClpC1P1P2. *Chem Biol* **21**, 509-518 (2014).
15. Choules MP, *et al*. Rufomycin targets ClpC1 proteolysis in *Mycobacterium tuberculosis* and *M. abscessus*. *Antimicrob Agents Chemother* **63**, e02204-18 (2019).
16. Schmitt EK, *et al*. The natural product cyclomarin kills *Mycobacterium tuberculosis* by targeting the ClpC1 subunit of the caseinolytic protease. *Angew Chem Int Ed Engl* **50**, 5889-5891 (2011).
17. Gao W, *et al*. The cyclic peptide ecumicin targeting ClpC1 is active against *Mycobacterium tuberculosis in vivo*. *Antimicrob Agents Chemother* **59**, 880-889 (2015).
18. Ma J, *et al*. Biosynthesis of ilamycins featuring unusual building blocks and engineered production of enhanced anti-tuberculosis agents. *Nat Commun* **8**, 391 (2017).
19. Shetye GS, Choi KB, Kim CY, Franzblau SG, Cho S. *In vitro* profiling of antitubercular compounds by rapid, efficient, and nondestructive assays using autoluminescent *Mycobacterium tuberculosis*. *Antimicrob Agents Chemother* **65**, e0028221 (2021).
20. Victoria L, Gupta A, Gómez JL, Robledo J. *Mycobacterium abscessus complex*: a review of recent developments in an emerging pathogen. *Front Cell Infect Microbiol* **11**, 659997 (2021).
21. Luthra S, Rominski A, Sander P. The role of antibiotic-target-modifying and antibiotic-modifying enzymes in *Mycobacterium abscessus* drug resistance. *Front Microbiol* **9**, 2179 (2018).
22. Stinear TP, *et al*. Insights from the complete genome sequence of *Mycobacterium*

marinum on the evolution of *Mycobacterium tuberculosis*. *Genome Res* **18**, 729-741 (2008).

23. Shiloh MU, Champion PAD. To catch a killer. What can mycobacterial models teach us about *Mycobacterium tuberculosis* pathogenesis? *Curr Opin Microbiol* **13**, 86-92 (2010).
24. Gutiérrez AV, Viljoen A, Ghigo E, Herrmann J-L, Kremer L. Glycopeptidolipids, a double-edged sword of the *Mycobacterium abscessus* complex. *Front Microbiol* **9**, 1145 (2018).
25. Jankute M, Grover S, Birch HL, Besra GS. Genetics of mycobacterial arabinogalactan and lipoarabinomannan assembly. *Microbiol Spectr* **2**, MGM2-2013 (2014).
26. Lu X, *et al.* Pyrazolo[1,5-]pyridine inhibitor of the respiratory cytochrome complex for the rreatment of drug-resistant tuberculosis. *ACS Infect Dis* **5**, 239-249 (2019).
27. Bergval I, *et al.* Pre-existing isoniazid resistance, but not the genotype of *Mycobacterium tuberculosis* drives rifampicin resistance codon preference *in vitro*. *PLoS One* **7**, e29108 (2012).
28. Wolf NM, *et al.* High-resolution structure of ClpC1-rufomycin and ligand binding studies provide a framework to design and optimize anti-tuberculosis Leads. *ACS Infect Dis* **5**, 829-840 (2019).
29. Wang S, *et al.* Amino acid 17 in QRDR of Gyrase A plays a key role in fluoroquinolones susceptibility in mycobacteria. *Microbiol Spectr* **11**, e0280923 (2023).
30. Yan M, Yan H, Ren G, Zhao J, Guo X, Sun Y. CRISPR-Cas12a-assisted recombineering in bacteria. *Appl Environ Microbiol* **83**, e00947-17 (2017).
31. Liu Y, *et al.* Assessment of clofazimine and TB47 combination activity against *Mycobacterium abscessus* using a bioluminescent approach. *Antimicrob Agents Chemother* **64**, e01881-19 (2020).
32. Yang F, *et al.* Engineering more stable, selectable marker-free autoluminescent mycobacteria by one step. *PloS One* **10**, e0119341 (2015).

33. Liu Y, *et al*. The compound TB47 is highly bactericidal against *Mycobacterium ulcerans* in a Buruli ulcer mouse model. *Nat Commun* **10**, 524 (2019).
34. Vasudevan D, Rao SP, Noble CG. Structural basis of mycobacterial inhibition by cyclomarin A. *J Biol Chem* **288**, 30883-30891 (2013).
35. Rifat D, Chen L, Kreiswirth BN, Nuermberger EL. Genome-wide essentiality analysis of *Mycobacterium abscessus* by saturated transposon mutagenesis and deep sequencing. *mBio* **12**, e0104921 (2021).
36. Bai J, Chi M, Hu Y, Hao M, Zhang X. Construction and biological vharacteristics of ClpC and ClpX knock-down strains in *Mycobacterium smegmatis*. *China Biotechnology* **41**, 13-22 (2021).
37. Pai MY, *et al*. Drug affinity responsive target stability (DARTS) for small-molecule target identification. *Methods Mol Biol* **1263**, 287-298 (2015).
38. Wojtyra UA, Thibault G, Tuite A, Houry WA. The N-terminal zinc binding domain of ClpX is a dimerization domain that modulates the chaperone function. *J Biol Chem* **278**, 48981-48990 (2003).
39. Ghanbarpour A, Fei X, Baker TA, Davis JH, Sauer RT. The SspB adaptor drives structural changes in the AAA+ ClpXP protease during ssrA-tagged substrate delivery. *Proc Natl Acad Sci U S A* **120**, e2219044120 (2023).
40. Dziedzic R, *et al*. *Mycobacterium tuberculosi*s ClpX interacts with FtsZ and interferes with FtsZ assembly. *PloS one* **5**, e11058 (2010).
41. Sklar JG, Makinoshima H, Schneider JS, Glickman MS. *M. tuberculosis* intramembrane protease Rip1 controls transcription through three anti□sigma factor substrates. *Mol Microbiol* **77**, 605-617 (2010).
42. Hameed HA, *et al.* Molecular targets related drug resistance mechanisms in MDR-, XDR-, and TDR-*Mycobacterium tuberculosis* strains. *Front Cell Infect* **8**, 114 (2018).
43. Unissa AN, Subbian S, Hanna LE, Selvakumar N. Overview on mechanisms of isoniazid action and resistance in *Mycobacterium tuberculosis*. *Infect Genet Evol* **45**, 474-492 (2016).
44. Ramaswamy SV, *et al.* Single nucleotide polymorphisms in genes associated

with isoniazid resistance in *Mycobacterium tuberculosis*. *Antimicrob Agents Chemother* **47**, 1241-1250 (2003).

45. Chen P, Bishai WR. Novel selection for isoniazid (INH) resistance genes supports a role for NAD+-binding proteins in mycobacterial INH resistance. *Infect Immun* **66**, 5099-5106 (1998).
46. Gao Y, *et al.* Ultra-short-course and intermittent TB47-containing oral regimens produce stable cure against Buruli ulcer in a murine model and prevent the emergence of resistance for *Mycobacterium ulcerans*. *Acta Pharm Sin B* **11**, 738-749 (2021).
47. Joshi AC, Kaur P, Nair RK, Lele DS, Nandicoori VK, Gopal B. Selectivity among anti-σ factors by *Mycobacterium tuberculosis* ClpX influences intracellular levels of extracytoplasmic function σ factors. *J Bacteriol* **201**, e00748-18 (2019).
48. Chhotaray C, *et al.* Comparative analysis of whole-genome and methylome profiles of a smooth and a rough *Mycobacterium abscessus* clinical strain. *G3 (Bethesda)* **10**, 13-22 (2020).
49. Zhang T, Li SY, Nuermberger EL. Autoluminescent *Mycobacterium tuberculosis* for rapid, real-time, non-invasive assessment of drug and vaccine efficacy. *PloS One* **7**, e29774 (2012).
50. Tian X, *et al.* Rapid visualized assessment of drug efficacy in live mice with a selectable marker-free autoluminescent *Klebsiella pneumoniae*. *Biosens Bioelectron* **177**, 112919 (2021).
51. Wang S, *et al.* Rapid, serial, non-invasive quantification of *Pseudomonas aeruginosa* in live mice with a selectable marker-free autoluminescent strain. *Biosens Bioelectron* **165**, 112396 (2020).
52. Yu W, *et al.* TB47 and clofazimine form a highly synergistic sterilizing block in a second-line regimen for tuberculosis in mice. *Biomed Pharmacother* **131**, 110782 (2020).
53. Liu P, *et al.* Design and synthesis of novel pyrimidine derivatives as potent antitubercular agents. *Eur J Med Chem* **163**, 169-182 (2019).

54. Morris GM, Huey R, Olson AJ. Using autodock for ligand receptor docking. *Curr Protoc Bioinformatics* **24**, 8.14. 11-18.14. 40 (2008).
55. Wang Y, *et al.* Pubchem bioassay: 2017 update. *Nucleic Acids Res* **45**, D955-D963 (2017).
56. Rock JM, *et al.* Programmable transcriptional repression in mycobacteria using an orthogonal CRISPR interference platform. *Nat Microbiol* **2**, 1-9 (2017).
57. Vivoli M, Novak HR, Littlechild JA, Harmer NJ. Determination of protein-ligand interactions using differential scanning fluorimetry. *J Vis Exp*, e51809 (2014).
58. Khadiullina R, Mirgayazova R, Davletshin D, Khusainova E, Chasov V, Bulatov E. Assessment of thermal stability of mutant p53 proteins via differential scanning fluorimetry. *Life (Basel)* **13**, 31 (2022).

Acknowledgments

We acknowledge the Yicheng Sun group from the Institute of Pathogenic Biology, Chinese Academy of Medical Sciences for kindly sending the pJV53-Cpf1 and pCR-Zeo plasmids as the tool of gene editing. This work was supported by the National Key R&D Program of China (2021YFA1300900), the National Natural Science Foundation of China (81973372, 32300152, 82022067, 22037006), China Postdoctoral Science Foundation (2022M723164), Guangdong Provincial Basic and Applied Basic Research Fund (2022A1515110505, 2019B030302004), the grant of State Key Lab of Respiratory Disease (SKLRD-Z-202414, SKLRD-Z-202301), Open Program of Shen Zhen Bay Laboratory (SZBL2021080601006) and Nansha District Science and Technology Plan Project (NSJL202102). The funders had no role in study design, data collection and analysis, decision to publish, or preparation of the manuscript.

Author contributions

T.Z., J.J., and X.X. supervised the project; T.Z., Y.G., and C.F. designed the whole project and most of the experiments; J.M. and C.S. prepared and characterized the ilamycin E and ilamycin F; Y.G. and C.F. performed the susceptibility testing and

resistant mutant screening; B.Z. and J.J. contributed to molecular docking simulation; C.F., X.T., and J.H. constructed overexpression and gene-editing strains and peformed the susceptibility testing; C.F. and X.H. performed the gene-scilencing experiments; Y.G. and B.Z. contributed to protein expression and mode of action experiments; C.F. and H.Z. contributed to the microscopy results; Y.G. performed the statistical analysis; Y.G., F.C., and T.Z. wrote the manuscript; H.M.A., J.M., X.C., N.Z., X.X., J.J., and T.Z. revised the manuscript.

Competing interests

The authors have no competing interests to declare that are relevant to the content of this article.